Evidence for extensive grain boundary meander and overgrowth of substrate grain boundaries in high critical current density ex situ $YBa_2Cu_3O_{7-x}$ coated conductors

D.M. Feldmann[a] and D.C. Larbalestier
Applied Superconductivity Center, University of Wisconsin–Madison, Madison, Wisconsin 53706

T. Holesinger
Los Alamos National Laboratory, Los Alamos, New Mexico 87545

R. Feenstra, A.A. Gapud, and E.D. Specht
Oak Ridge National Laboratory, Oak Ridge, Tennessee 37831

(Received 17 January 2005; accepted 19 April 2005)

It has been generally accepted that $YBa_2Cu_3O_{7-x}$ (YBCO) films deposited on deformation textured polycrystalline metal tapes result in YBCO grain boundary (GB) networks that essentially replicate the GBs of the underlying substrate. Here we report that for thicker YBCO films produced by a BaF_2 ex situ process, this is not true. Using electron backscatter diffraction combined with ion milling, we have been able to map the evolution of the YBCO grain structure and compare it to the underlying template in several coated conductors. For thin ($\leqslant$0.5 μm) YBCO films deposited on rolling-assisted biaxially textured substrates (RABiTS), the YBCO GBs nearly directly overlap the substrate GBs. For 0.7–1.4 μm YBCO films, the GBs were found to meander along the substrate GBs and along the sample normal, with displacements several times the film thickness. In very thick films (2.5–2.9 μm), the YBCO grains can completely overgrow substrate grains and GBs, resulting in a substantial disconnection of the YBCO and substrate GB networks. Similar behavior is found for BaF_2 ex situ YBCO films on ion-beam-assisted deposition-type templates. The ability of the YBCO to overgrow substrate grains and GBs is believed to be due to liquid-phase mediated laminar grain growth. Although the behavior of the YBCO GB networks changes with YBCO film thickness, the samples maintained high critical current density (J_c) values of >2 MA/cm^2 for films up to 1.4 μm thick, and up to 0.9 MA/cm^2 for 2.5–2.9-μm-thick films.

I. INTRODUCTION

One approach to the development of practical high temperature superconducting (HTS) wires is to deposit epitaxial $YBa_2Cu_3O_{7-x}$ (YBCO) on oxide buffered flexible metal tapes.[1–4] Cost-effective commercial production of these coated conductors (CCs) will require large critical currents (I_c) and fast YBCO growth processes. The latter requirement may be met by the ex situ conversion of YBCO precursors,[5–9] metalorganic chemical vapor deposition,[10,11] or pulsed laser deposition methods.[12] A recent electromechanical study of CCs suggests that YBCO layers up to 3 μm thick meet the strain requirements of most applications.[13] The strong dependence of the critical current density (J_c) of YBCO with grain boundary (GB) misorientation angle[14–17] also requires CC templates with excellent biaxial texture. The long, flexible, metal-based templates used to support the epitaxial oxide growth of the buffer and superconducting films are typically based either on ion-beam-assisted deposition (IBAD) of a biaxially oriented oxide layer on a randomly oriented polycrystalline metal strip,[2,12,18,19] or a biaxially textured metal strip produced by the rolling assisted biaxially textured substrates (RABiTS) process.[20]

In the ex situ process, YBCO films are converted in a furnace using BaF_2-based precursors that may be deposited onto suitable substrates by either physical vapor deposition (PVD)[6,21,22] or metal organic deposition (MOD).[7,9] The ex situ method is an economically attractive process for the commercial production of CCs, capable of producing YBCO films at high conversion rates with high critical current densities.[22–24] A recent microstructural study has revealed that films produced by the PVD-BaF_2 method are characterized by a laminar grain structure resulting from the anisotropic growth characteristics of YBCO and liquid-phase mediated grain

[a]Address all correspondence to this author.
e-mail: feldmann@cae.wisc.edu
DOI: 10.1557/JMR.2005.0262

 © 2005 Materials Research Society

growth during precursor conversion.[25] Such films may also exhibit a bimodal microstructure, with very large, well-formed grains in the bottom half of the film, and small grains in the top. Grains in excess of 50 μm in size were observed in the bottom half of a 2.9-μm-thick YBCO film on an IBAD-yttria-stabilized zirconia (YSZ) template, where the YSZ grain size was 0.1–0.25 μm.[25] The anisotropic, liquid-phase mediated grain growth allowed the YBCO grains to overgrow many substrate grains and GBs. YBCO GBs resulting from GBs in the underlying substrate were observed to meander significantly through the film thickness, an achievement also believed to be facilitated by liquid-mediated grain growth.[25]

Previous magneto-optical studies of YBCO CCs revealed that current percolates through the conductors due to J_c variations among the grains and GBs.[1,26,27] In those studies, the YBCO films were either produced by pulsed laser deposition (PLD), or were produced by the PVD-BaF_2 method and were less than 0.4 μm thick. For both deposition methods, the scale of the YBCO GB networks was essentially determined by the substrate for both IBAD and RABiTS-type templates. In the case of RABiTS, the YBCO GB networks were found to overlap the substrate GB networks nearly exactly.[26,27] This is the anticipated result for epitaxial YBCO growth. However, the 50-μm YBCO grain size observed in thick PVD-BaF_2 processed film on an IBAD-YSZ template is a significant deviation from the texture template.[25]

In an effort to optimize J_c in thick ex situ processed films, understanding changes in the YBCO GB networks as a function of film thickness and the impact on current flow is of great interest. In this paper, YBCO GB networks are compared to the underlying substrate GBs in both IBAD and RABiTS-type CCs for PVD-BaF_2 processed films 0.5–2.9 μm thick.

II. EXPERIMENTAL

All YBCO films in this work were grown by the physical vapor deposition (PVD) of a BaF_2-based precursor and subsequent ex situ anneal. Details of the ex situ conversion of the PVD BaF_2-based precursors in this work are given elsewhere.[22] Briefly, precursor layers of the desired thickness were prepared by vacuum deposition using three electron-beam sources (Y, BaF_2, and Cu) onto a substrate at 100 °C. The precursors were converted into epitaxial YBCO by annealing in a furnace under flowing gas conditions at atmospheric pressure. Maximum temperatures during the anneal reached 780 °C. The precursors were converted to YBCO at ~1–5 Å/s. The oxygen partial pressure was 250 mTorr, and the water partial pressure (needed to decompose incorporated BaF_2 of the precursor layer) was kept below 15 Torr. YBCO films were deposited on both RABiTS and Hastelloy substrates buffered with IBAD-YSZ. The structure of the IBAD-YSZ samples was YBCO (1.1–2.9 μm)/CeO_2 (15–30 nm)/YSZ (1.0 μm)/Hastelloy (100 μm) and the structure of the RABiTS samples was YBCO (0.5–2.5 μm)/CeO_2 (15–40 nm)/YSZ (150–200 nm)/Y_2O_3 (30–50 nm)/Ni–5 at.%W (75 μm) or Ni–3 at.%W (50 μm). Full width at half-maximum (FWHM) in-plane and out of plane values for the YBCO on IBAD-YSZ were respectively 7.9° and 3.5–5.2°. Typical texture values for YBCO on RABiTS were in-plane (true $\Delta\Phi$) ~ 4.7–6.5° and 5.1–6.8° out-of-plane. The variation in these values is partly due to texture differences between the Ni–W substrates;[22] however, the FWHM values also increase with the YBCO thickness.[25]

Electron back-scatter diffraction (EBSD) was used to produce spatially resolved maps of crystal orientation, where the map normal is parallel to the sample normal. EBSD was performed in a field emission scanning electron microscope (FESEM) at a 70° sample tilt. Data was taken on a hexagonal grid with varying step sizes in the range of ~0.2–1.0 μm. Scan size was 180 × 200 μm or greater and scans contained between 5×10^4 and 1.4×10^5 data points. The spatial resolution (or effective volume of material sampled) of EBSD is difficult to quantify and depends on several factors, including material and electron beam conditions. For a detailed discussion, see Goyal et al.[28] or Humphreys.[29] In this work the resolution is ~0.2–0.6 μm in the plane and <0.2 μm in depth. Transmission and scanning transmission electron microscopy (TEM/STEM) was used to image the GB meandering and overgrowth in cross section. A Tecnai TF30 TEM/STEM microscope (FEI Company, Hillsboro, OR) operating at 300 kV was used for this work.

To track the grain structure and GB geometry of the CC samples through thickness, EBSD and ion milling were used successively. A Nd-YAG laser operating at an average power of 8 mW was used to define the region for the scans. The laser cuts penetrated through the YBCO and buffer layers into the substrate, providing spatial registration of multiple EBSD scans through thickness. After the initial EBSD scan, samples were thinned by ion milling and another scan performed (Fig. 1). In some cases, this procedure was repeated several times on one sample, and in this way the crystal orientations and GB networks of the substrate, buffer layers, and YBCO could be compared in the same location. The ion milling occurred at ~250 K with argon ions of energy 500 eV. The ions impacted the samples at 45° to the sample normal and the etch rate for the YBCO was ~10 nm/min. A previous through-thickness J_c study of thick ex situ films strongly suggested that the ion milling procedure did not damage the films.[30]

III. RESULTS

Using the procedure outlined above, the GB networks of a 0.5-μm-thick YBCO film on RABiTS [J_c(77 K, 0 T)

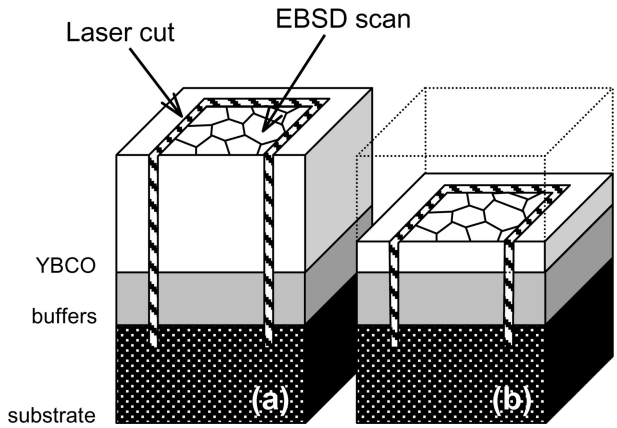

FIG. 1. The experimental geometry used in this work to align several 2D EBSD scans through thickness is shown in (a) and (b). An EBSD scan is performed on the surface of the sample (a), and then again after removal of material by ion milling (b). This procedure may be repeated several times. Laser cuts provide registration of the EBSD scans through thickness.

$= 2.1$ MA/cm^2] were mapped in both the YBCO and the underlying NiW substrate. Figures 2(a) and 2(b) present all GBs in the YBCO and NiW, respectively, with total misorientation angle (θ) $\geqslant 2°$. Figure 2(c) is an overlay of the YBCO GBs onto the NiW GBs. It can be seen that all the GBs in the YBCO are correlated to GBs in the substrate, and the two maps are essentially overlapping. This near duplication of the substrate GB network by the YBCO is typical of thin ($\leqslant$0.5 μm) ex situ films, and has also been observed in YBCO films up to 1.2 μm thick grown in situ by pulsed laser deposition (PLD) on RABiTS-type substrates.[26,27]

In a 1.0-μm-thick YBCO film on RABiTS [J_c(77 K, 0 T) $= 2.4$ MA/cm^2], a different behavior for the GB network was found. For this sample, EBSD scans were taken at YBCO thicknesses of 0.8, 0.5, and 0.2 μm, and in the underlying YSZ buffer layer and in the NiW substrate. Figures 3(a) and 3(b) are GB maps (all GBs $\geqslant 2°$) of the NiW and YSZ, respectively. (Note that these maps were generated after collection of the YBCO data). Figure 3(c) overlays the YSZ GB map onto the NiW GB map, and they overlap nearly exactly.

Figure 3(d) presents the GB map (all GBs $\geqslant 2°$) in the YBCO at a thickness of 0.2 μm (after 0.8 μm of the YBCO has been milled away). The substrate grain structure is recognizable in the YBCO GB map, but when the YBCO GB map is overlayed onto the NiW and YSZ GB maps [Fig. 3(e)], it can be seen that the YBCO GBs do not directly overlap the substrate GBs as was observed in the 0.5-μm film. In this case, the YBCO GBs are "wavy," meandering along the substrate GBs. The meandering GBs may also be spatially shifted away from the substrate GBs, as highlighted by the arrows [Fig. 3(e)].

Figure 3(f) is an overlay of, from front to back, the GB network in the YBCO at 0.8 μm (red), 0.5 μm (green), 0.2 μm, (blue), and the NiW (black). The YBCO GB networks, which do not directly overlap the substrate GBs, also do not directly overlap each other. This indicates that the YBCO GBs are also meandering through the film thickness, and that the GB planes are not parallel to the sample normal. Figure 3(g) highlights one example of GB meandering in the plane of the film. This example illustrates the general trend for the greatest degree of meandering to occur in the top (red) of the film. Likening the meandering GB to a wave, the amplitude of the meander in the top of the film is more than 10× the film thickness. In Fig. 3(h), the GB in the YBCO is found to be progressively shifted away from the substrate GB as the GB is traversed from bottom to top through the film. From the length marker in Fig. 3(h), it can be seen that the GB in the YBCO has shifted more than 15 μm through the film thickness of less than 1 μm. Figures 3(i)–3(k) present the GB networks for the same 1.0-μm film, this time color-coded by total misorientation angle (θ). For a given GB, the θ in the YBCO is typically similar to the θ in the YSZ. Also, θ does not

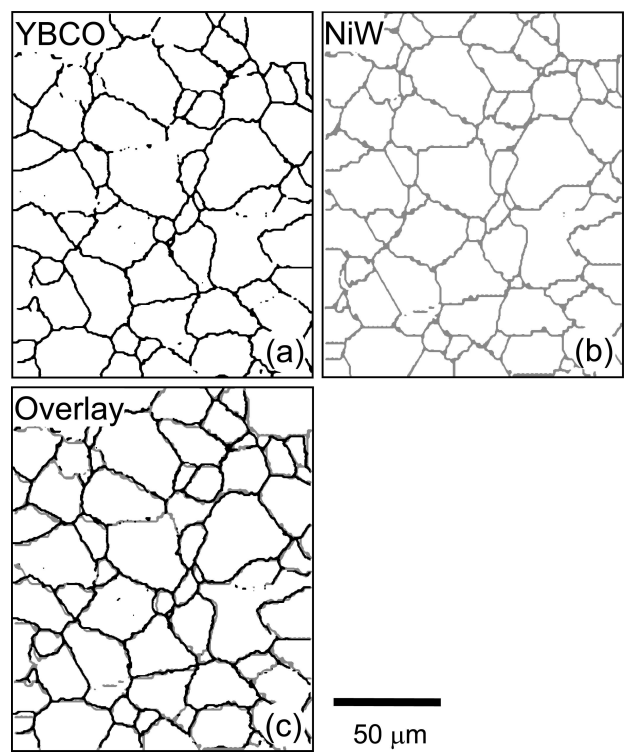

FIG. 2. Grain boundary maps for the (a) YBCO and (b) underlying NiW substrate in a RABiTS-type CC with a YBCO layer thickness of 0.5 μm [J_c(77 K, 0 T) $= 2.1$ MA/cm^2]. Shown are all GBs with $\theta \geqslant 2°$. The YBCO GB map was obtained at a thickness of 0.45 μm after milling just 0.05 μm from the film surface. From the overlay (c) of the YBCO GB map onto the NiW GB map it can be seen that the YBCO GBs essentially line up with substrate GBs. GBs that appear in the NiW but are absent in the YBCO map have a θ below the artificially imposed 2° cut-off.

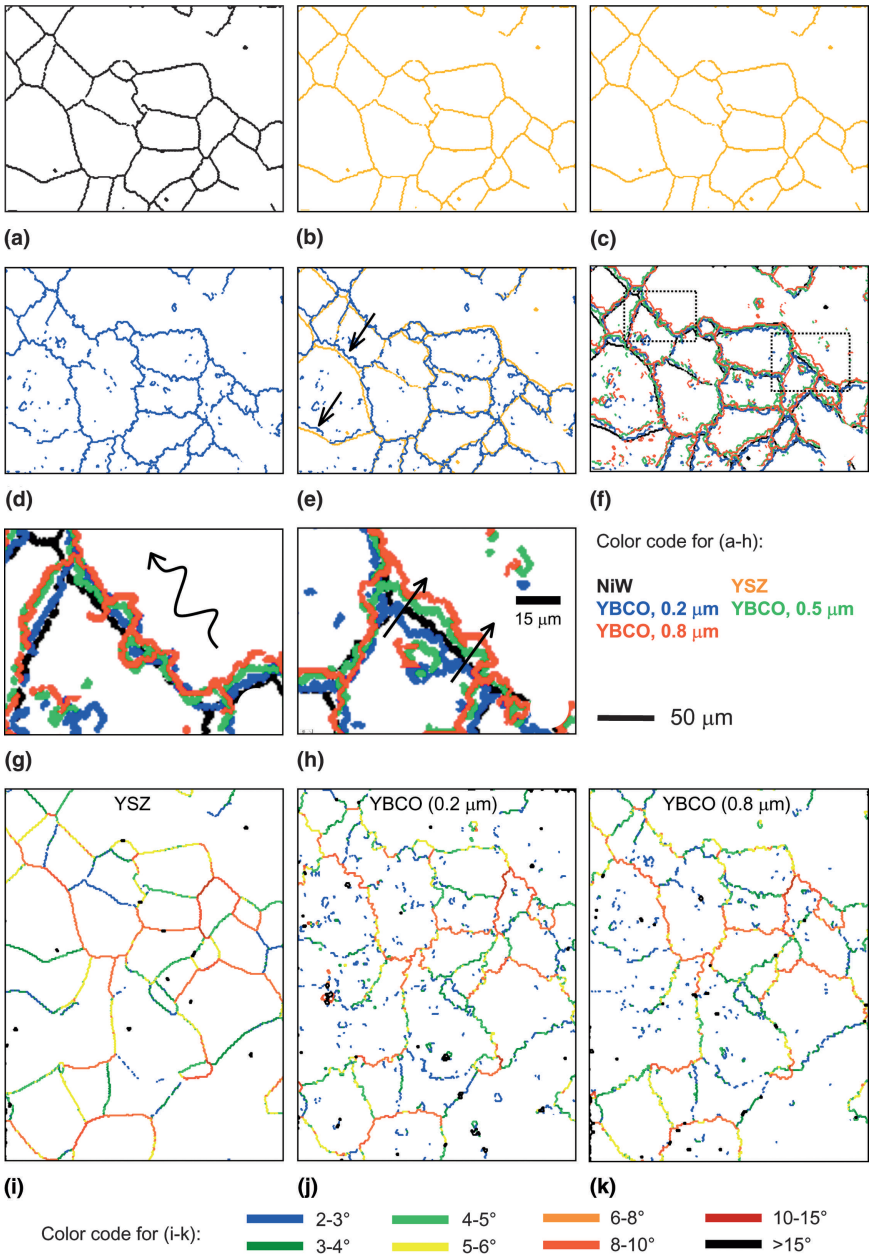

FIG. 3. Grain boundary maps throughout the thickness of a RABiTS-type CC with a 1.0 μm YBCO layer [J_c(77 K, 0 T) = 2.4 MA/cm^2]. For (a–h), GBs are color coded by layer, and in each layer all GBs with $\theta \geqslant 2°$ are shown. (a) NiW, (b) YSZ, (c) YSZ overlayed onto the NiW, (d) YBCO at 0.2 μm from the buffer interface, (e) overlay of YBCO map at 0.2 μm onto the YSZ map, (f) overlay of, from front to back, the YBCO GBs at 0.8, 0.5, and 0.2 μm and the NiW, (g) an example of YBCO GB meandering with respect to the substrate GB, (h) an example of a GB meandering through the film thickness. For (i–k), the GBs are color coded according to θ. GBs with $\theta \leqslant 2°$ are not shown: (i) YSZ, (j), YBCO at 0.2 μm from the buffer interface, and (k) YBCO at 0.8 μm from the buffer interface. The 50-μm length marker applies to (a–f) and (i–k).

change significantly through the thickness of the YBCO layer.

It should be emphasized that the observed GB meandering in the YBCO is reproducible under different scan conditions and is not an artifact of noise in the data, poor Kikuchi pattern quality, or indexing. Two EBSD scans performed in the same area on a 1.0-μm-thick YBCO film on RABiTS, one with a 40% smaller step size and 70% smaller volume of YBCO sampled at each point, exhibited nearly identical GB meandering. The quality (signal to noise ratio) of the Kikuchi patterns obtained from the 1.0-μm-thick YBCO films were similar to those obtained from the 0.5-μm-thick film.

A previous study has shown GB meandering in a 1.4-μm-thick PVD-BaF_2 processed film on RABiTS.[25] In this study, both YBCO GB overgrowth and meandering have been observed by EBSD in YBCO films of 0.7–1.4 μm.[31] A cross-sectional TEM image from a

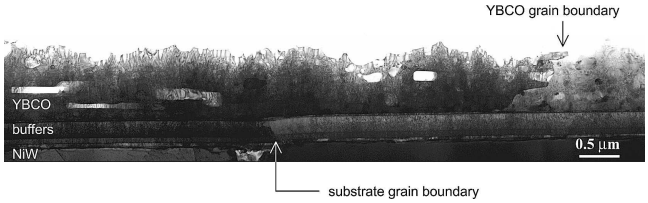

FIG. 4. A cross-section TEM image of a 1.25-μm-thick YBCO film on RABiTS [J_c(77 K, 0 T) = 2.7 MA/cm^2] showing a substrate GB and corresponding GB in the YBCO. The YBCO has overgrown the substrate GB by several microns, and the YBCO GB meanders through the thickness of the film.

RABiTS-type CC with a 1.25-μm-thick YBCO layer [J_c(77 K, 0 T) = 2.7 MA/cm^2] showing both the overgrowth and meandering is shown in Fig. 4. The substrate GB and corresponding GB in the YBCO are highlighted by diffraction contrast. The left and right YBCO grains are aligned with the left and right substrate grains, respectively. However, the left YBCO grain has overgrown the substrate GB by >2.5× the film thickness, and the YBCO GB meanders through thickness, shifting laterally by more than 1 μm from the bottom to the top of the film. At the surface of the film, the YBCO GB is estimated to be displaced by more than 4 μm from the substrate GB.

Figure 5 presents data similar to Fig. 2 for two RABiTS-type CC samples, each with a 2.5-μm-thick YBCO layer. These thick ex situ processed films are characterized by a "bimodal" microstructure, with large well-formed YBCO grains in the bottom of the film, and much smaller grains in the top of the film.[25,30] The YBCO grains in the bottom of the bimodal microstructure are typically 0.2 to >1 μm thick. For the data of Fig. 5, both YBCO films were ion milled to a thickness of 0.2 μm to remove the small-grain material and reveal the large grain material closest to the buffer interface. For the film shown in Figs. 5(a)–5(c) [J_c(77 K, 0 T) = 0.6 MA/cm^2], it can be seen that there is a substantial discrepancy between the YBCO and NiW GB networks. While there are some YBCO GBs that appear to be correlated to substrate GBs, there are more that appear to have no correlation. The numbered arrows in Fig. 5(c) highlight examples of substrate GBs in the middle of a YBCO grain (1), YBCO GBs in the middle of a substrate grain (2), and a YBCO GB that can be correlated to a

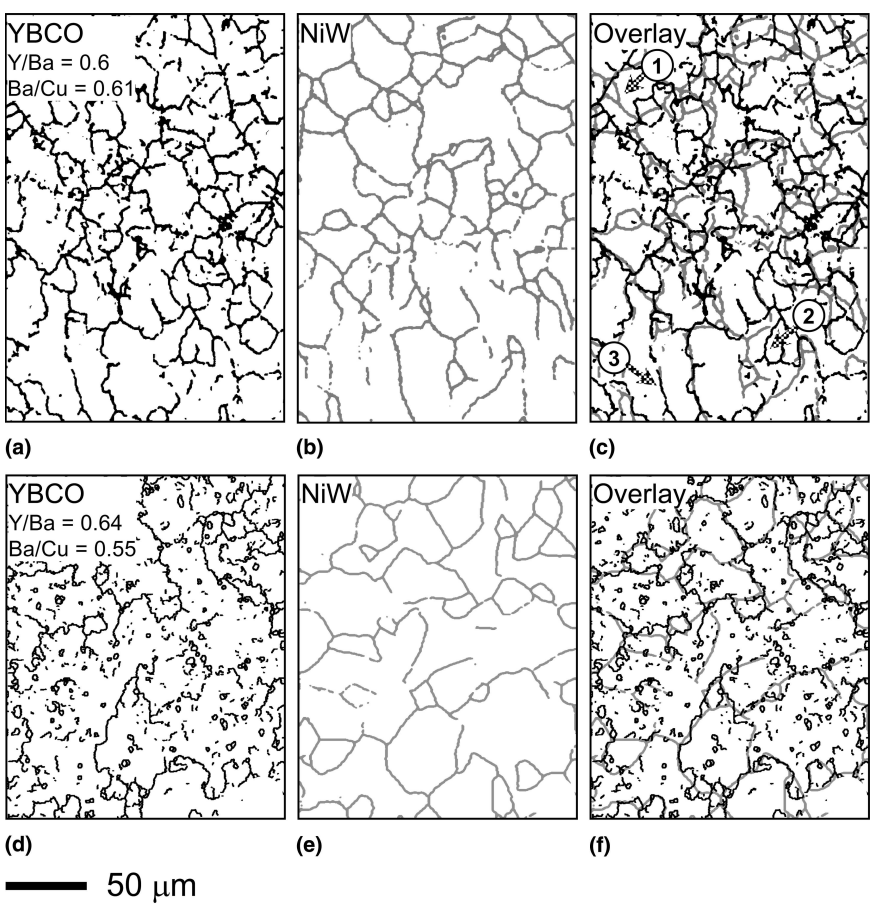

FIG. 5. Grain boundary maps for the YBCO and underlying NiW substrate in two different RABiTS-type CCs with a YBCO layer thickness of 2.5 μm. Shown are all GBs with θ ⩾ 2°. The YBCO GB map was obtained at a thickness of 0.2 μm for both samples, after milling 2.3 μm from the film surface. For the first sample [J_c(77 K, 0 T) = 0.6 MA/cm^2]: (a) YBCO, (b) NiW, and (c) overlay of the YBCO onto the NiW. For the second sample [J_c(77 K, 0 T) = 0.9 MA/cm^2]: (d) YBCO, (e) NiW, and (f) overlay of the YBCO onto the NiW.

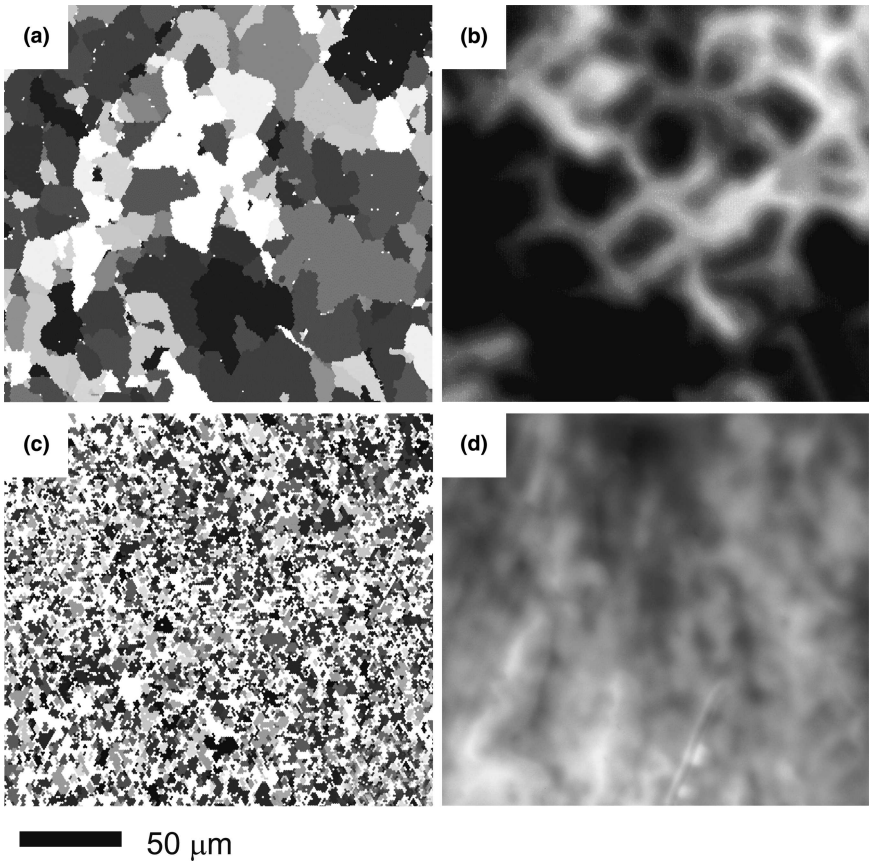

FIG. 6. Unique grain maps and magneto-optical images from 1.1- and 2.9-μm-thick YBCO layers on IBAD-YSZ. Colors in the map do not reflect orientation. For the 2.9-μm sample [J_c(77 K, 0 T) = 0.9 MA/cm^2]: (a) grain map and (b) magneto-optical image. For the 1.1-μm sample [J_c(77 K, 0 T) = 1.7 MA/cm^2]: (a) grain map and (b) magneto-optical image.

substrate GB (3). Figures 5(d)–5(f) present the second 2.5-μm sample [J_c(77 K, 0 T) = 0.9 MA/cm^2]. For this film, there is a stronger correlation between the YBCO and substrate GB networks. In many cases, the YBCO GBs appear to meander along the substrate GBs, as in the case of the 1.0-μm-thick film, but here the spatial scale (amplitude and wavelength) of the meandering is larger. There is also a "subgrain" structure in the YBCO, appearing as many small round grains within a larger grain. EBSD revealed that these subgrains have poor *c*-axis alignment. Since both films were reacted from precursors of the same thickness, the observed differences in the behavior of the GB networks may be attributed to other parameters. Both films were annealed under similar conditions (~1 Å/s conversion rate), but the precursor compositions [expressed in ratios of the constituents in Fig. 5 (Y/Ba and Ba/Cu)] were significantly different.

Strong changes in the YBCO GB networks as a function of film thickness are not unique to RABiTS-type CCs and have been observed in IBAD-YSZ CCs as well. We previously reported a bimodal microstructure in a 2.9-μm-thick YBCO film on IBAD-YSZ [J_c(77 K, 0 T) = 0.9 MA/cm^2].[25,30] This YBCO film was ion milled to a thickness of 0.9 μm, exposing the large grain material. An EBSD scan after ion milling, Fig. 6(a), revealed a very large YBCO grain size of 30–50 μm.[25] This is to be compared to the IBAD-YSZ grain size of ~0.1–0.25 μm, shown in the cross-sectional TEM image of Fig. 7, where a single YBCO grain has overgrown several YSZ grains. The electromagnetic consequences

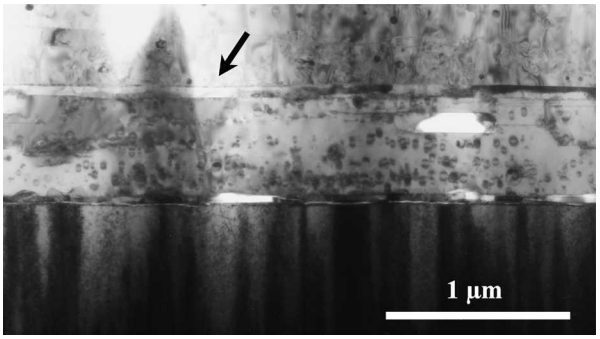

FIG. 7. Cross-sectional TEM image of a 2.9-μm YBCO film on IBAD-YSZ [J_c(77 K, 0 T) = 0.9 MA/cm^2]. Two large YBCO grains are separate by a second phase layer, highlighted with an arrow. The YBCO grains extend beyond the edges of the image in both directions, and can be seen to overgrow many buffer layer grains, which exhibit a columnar structure.

of the large YBCO grain structure can be seen in Fig. 6(b), which shows a magneto-optical image of the same film, taken after milling to 0.9 μm. For this image the sample was zero-field cooled to 77 K, and then a field of 60 mT was applied. The result is a strongly inhomogeneous flux penetration with a magnetic granularity of ~50 μm, more closely resembling flux penetration of a thin film on RABiTS than a thin film on an IBAD-type CC. For contrast a 1.1-μm-thick YBCO film [J_c(77 K, 0 T) = 1.7 MA/cm^2] on IBAD-YSZ is shown in Figs. 6(c) and 6(d). The EBSD data [Fig. 6(c)] shows a significantly smaller YBCO grain size, more consistent with the substrate grain size. The magneto-optical image of this film [Fig. 6(d)] also reveals granularity more consistent with the substrate grain size and very similar to magneto-optical images of thinner YBCO films on IBAD-YSZ substrates.[1,32] The small grain size of the IBAD-YSZ samples make GB meandering difficult to observe by EBSD if present. Cross-section TEM images of the 1.1-μm-thick film revealed isolated, larger YBCO grains <5 μm size in the bottom of the film but did not reveal a continuous layer of large grain material (associated with a bimodal microstructure).

IV. DISCUSSION

Experimentally, we have observed very different behaviors of the YBCO GB networks of the PVD-BaF_2 processed films as a function of YBCO film thickness. The traditional scenario observed for both PLD and thin (≤0.5 μm) ex situ processed thin films, where the YBCO GB networks are strongly driven by the texture template in both IBAD and RABiTS-type CCs,[1,26,27] does not hold for thicker ex situ films. YBCO GB meandering occurs in 0.7–1.4-μm-thick films, both along the substrate GBs (in the plane of the film) and through the film thickness. Complete substrate grain overgrowth and a very large YBCO grain size of 30–50 μm occur in 2.5–2.9-μm-thick films. Holesinger et al. has demonstrated that a transient liquid phase is present in these PVD-BaF_2 films during conversion,[25] which is believed to be responsible for the deviation of the YBCO GBs from the texture template.

The bimodal microstructure frequently seen in thick PVD-BaF_2 processed films has been concluded to be the result of YBCO precipitation from a transient liquid phase due to slightly different reaction routes.[25] The 2.5–2.9-μm-thick films of this study had a bimodal microstructure and large deviations between the YBCO and substrate GB networks of these films (Fig. 5), consisting of YBCO grains overgrowing substrate GBs by tens of microns in only the bottom 0.2 μm of the film, adds further evidence of grain growth in the presence of a liquid phase. The 1.0 and 1.25 μm films of this study did not exhibit a bimodal microstructure but are also believed to be the result of liquid-assisted growth. For the 1.0-μm-thick film, the YBCO GBs meander along the substrate GBs with an amplitude of several microns to more than 10× the film thickness, and may even be shifted away from the substrate GBs, as seen in several GBs in Fig. 3. The cross-sectional TEM image of Fig. 4 reveals a remarkable result of YBCO growth in a 1.25-μm film; a YBCO grain has overgrown a substrate GB by more than 2.5 μm, and the associated YBCO GB meanders significantly through thickness. These observations also strongly suggest the presence of a liquid phase during conversion. TEM observations of defect structures and second phases suggest that a liquid phase may be present even at 0.5 μm,[33] though no evidence for a liquid phase can be discerned at the resolution of EBSD at that thickness. It is likely a liquid phase is always present during the conversion of these films, and the amount of the liquid phase increases with precursor thickness. The increasing amount of liquid allows for increasing dissociation of the YBCO GB networks from the texture templates.

GB meandering has previously been observed by plan-view TEM in thin PLD YBCO films.[34,35] On the smallest scales, changes in the faceting along a GB may be considered GB meandering. Zhang et al. reported an average meander amplitude of ~0.15 μm with peaks up to 0.4 μm in a thin PLD YBCO film on a 36° [001] tilt $SrTiO_3$ (STO) substrate.[34] In the PVD-BaF_2 films, the scale of the GB meandering is considerably greater, peaking at more than 10× the film thickness in a 1-μm film. Zhang et al. attributed meandering GBs in PLD films to an island growth mechanism, while in the ex situ films, the liquid-phase mediated laminar grain growth allows for a much greater amplitude of GB meandering and substrate grain overgrowth. Zhang et al. also observed shifting of a meandering YBCO GB away from the substrate GB, as seen in several GBs in Fig. 3. It was speculated that surface morphology or *c*-axis tilting of the STO substrate grains was responsible. The [001] direction of the individual grains of RABiTS are frequently observed to be in the range 0–10°, significantly greater than that typically encountered in manufactured bicrystal substrates. In the EBSD data of the 1.0-μm film of this study, there was no clear correlation between *c*-axis tilting of the substrate grains and shifting of the YBCO GB away from the substrate GB. We also found no correlation between the *c*-axis tilting of the substrate grains and the YBCO GB meander amplitude. Figure 8 shows EBSD data from a 1.0-μm-thick PVD-BaF_2 YBCO film grown on a 5° [001] tilt YSZ bicrystal substrate. The meander of this YBCO GB is very similar to that observed in the 1.0-μm film on RABiTS, even though the [001] deviates from the surface normal of the STO substrate by only 0.5°, significantly less than is typically observed for grains in

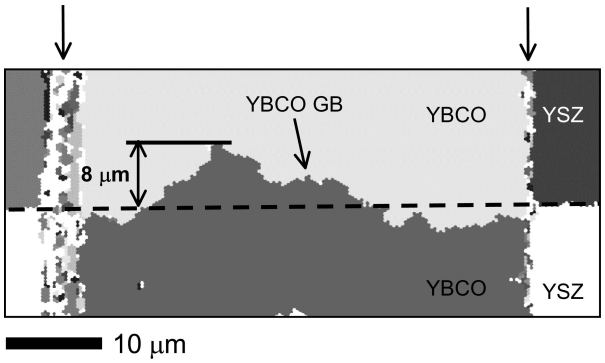

FIG. 8. Unique grain map of a 50-μm-wide trace patterned in a 1.0-μm YBCO film on a 5° [001] tilt YSZ bicrytstal substrate [J_c(77 K, 0 T) = 1.4 MA/cm^2]. Colors in the map do not reflect orientation. The YSZ is exposed on either side of the link. The YSZ GB is straight, and its position is marked with a horizontal dashed line. Two vertical strips of noise occur in the scan at the YBCO trace edges, marked with arrows at the top of the figure. The YBCO GB exhibits a large degree of meander, with amplitude up to 8 μm.

RABiTS. Since the meander in the ex situ films is a result of liquid-assisted laminar grain growth, the mechanisms controlling the amplitude of the meander and overgrowth of substrate GBs are probably not the same as in PLD films.

Zhang et al. noted that as a consequence of GB meander, the area of the GB is increased, which may yield an increase in I_c.[34] A recent bicrystal study, which varied the area of the GB within a transport link by changing the angle between the link and the GB, demonstrated this effect.[36] However, that study may be too simplistic to apply to meandering GBs, as the faceting of the GB remained unchanged. A meandering GB probably introduces a change in faceting along the GB as well, and how transport properties vary with facet structure in YBCO GBs is not completely understood. It is also important to note that due to the less-than-perfect biaxial texture of CCs, the facet structure of CC GBs may be more complex than that observed in PLD films on [001] tilt bicrystal substrates. Durrell et al. found that when the vortices were rotated out of the plane of the GB, segments of the vortex became strongly pinned in the bulk, allowing the GB to carry a larger transport current.[37] In Fig. 3(h), a GB meanders through thickness, with the GB plane making a very low angle with the plane of the film. It is possible that in such situations, the conditions of the Durrell et al. experiment are satisfied, and segments of the GB vortices become strongly pinned in the bulk, enhancing I_c. A recent study of MOD processed CCs, where the width of a transport link was successively reduced, suggested that the GBs of those CCs exhibited a J_c higher than would be expected from thin film bicrystal studies.[38] Transport measurements of meandering GBs in thicker ex situ processed films are under investigation and will be published at a later date.

V. SUMMARY

The results of the PVD-BaF_2 films of this work may be summarized as follows.

In thin YBCO films (≤0.5 μm), the YBCO GBs are essentially "straight," replicating the profile of the substrate GBs.

In YBCO films ~1.0–1.4 μm thick, the YBCO GBs meander along the substrate GBs and through the film thickness. The YBCO can overgrow the substrate GBs, shifting the YBCO GB away from the substrate GB.

In YBCO films ~2.5–2.9 μm thick, the YBCO grains can completely overgrow substrate grains and GBs, and there may be a substantial dissociation of the YBCO and substrate GB networks. YBCO GB meandering and very large YBCO grain size of >50 μm was observed.

A previous TEM-based study concluded that such films are characterized by YBCO grain growth from a transient liquid phase, and the meandering and substrate grain overgrowth observed here also strongly suggest the presence of a liquid phase. Further studies are needed to understand the electromagnetic implications of this newly observed behavior of the GB networks in thick PVD-BaF_2 processed films.

ACKNOWLEDGMENTS

DMF would like to thank Matt Nowell (Ametek Corporation, Paoli, PA) for experimental assistance. We express thanks to P. Arendt (Los Alamos National Laboratory, Los Alamos, NM) and American Superconductor Corporation for providing substrates. This work was funded by the U.S. Department of Energy (DOE) and the Air Force Office of Scientific Research (AFOSR).

REFERENCES

1. D. Larbalestier, A. Gurevich, D.M. Feldmann, and A. Polyanskii: High-T-c superconducting materials for electric power applications. *Nature* **414,** 368 (2001).
2. P.N. Arendt and S.R. Foltyn: Biaxially textured IBAD-MgO templates for YBCO-coated conductors. *MRS Bull.* **29**(8), 543 (2004).
3. Y. Iijima, K. Kakimoto, Y. Yamada, T. Izumi, T. Saitoh, and Y. Shiohara: Research and development of biaxially textured IBAD-GZO templates for coated superconductors. *MRS Bull.* **29**(8), 564 (2004).
4. A. Goyal, M.P. Paranthaman, and U. Schoop: The RABiTS approach: Using rolling-assisted biaxially textured substrates for high-performance YBCO superconductors. *MRS Bull.* **29**(8), 552 (2004).
5. A. Gupta, R. Jagannathan, E.I. Cooper, E.A. Giess, J.I. Landman, and B.W. Hussey: Superconducting oxide-films with high transition-temperature prepared from metal trifluoroacetate precursors. *Appl. Phys. Lett.* **52,** 2077 (1988).
6. R. Feenstra, T.B. Lindemer, J.D. Budai, and M.D. Galloway: Effect of oxygen-pressure on the synthesis of $YBa_2Cu_3O_{7-X}$ thin-films by post deposition annealing. *J. Appl. Phys.* **69,** 6569 (1991).
7. P.C. Mcintyre and M.J. Cima: Heteroepitaxial growth of chemically derived ex-situ $Ba_2YCu_3O_{7-X}$ thin-films. *J. Mater. Res.* **9,** 2219 (1994).

8. V.F. Solovyov, H.J. Wiesmann, L.J. Wu, M. Suenaga, and R. Feenstra: High-rate deposition of 5-mu-m thick $YBa_2Cu_3O_7$ films using the BaF_2 ex-situ post annealing process. *IEEE Trans. Appl. Supercond.* **9,** 1467 (1999).
9. X. Li, M.W. Rupich, W. Zhang, N. Nguyen, T. Kodenkandath, U. Schoop, D.T. Verebelyi, C. Thieme, M. Jowett, P.N. Arendt, S.R. Foltyn, T.G. Holesinger, T. Aytug, D.K. Christen, and M.P. Paranthaman: High critical current MOD ex situ YBCO films on RABiTS (TM) and MgO-IBAD templates. *Physica C* **390,** 249 (2003).
10. V. Selvamanickam, H.G. Lee, Y. Li, J. Reeves, Y. Qiao, Y.Y. Xie, K. Lenseth, G. Carota, M. Funk, K. Zdun, J. Xie, K. Likes, M. Jones, L. Hope, and D.W. Hazelton: Scale up of high-performance Y-Ba-Cu-O coated conductors. *IEEE Trans. Appl. Supercond.* **13,** 2492 (2003).
11. S. Donet, F. Weiss, P. Chaudouet, S. Beauquis, A. Abrutis, H.C. Freyhardt, A. Usokin, D. Selbmann, J. Eickemeyer, C. Jimenez, C.E. Bruzek, and J.M. Saugrain: Reel-to-reel MOCVD for YBCO coated conductor. *IEEE Trans. Appl. Supercond.* **13,** 2524 (2003).
12. S.R. Foltyn, P.N. Arendt, P.C. Dowden, R.F. DePaula, J.R. Groves, J.Y. Coulter, Q.X. Jia, M.P. Maley, and D.E. Peterson: High-T_c coated conductors—Performance of meter-long YBCO/IBAD flexible tapes. *IEEE Trans. Appl. Supercond.* **9,** 1519 (1999).
13. J.W. Ekin: Electromechanical studies for superconductor development, in *Superconductivity for Electric Systems 2004* Annual Peer Review (Washington, DC, 2004).
14. D.T. Verebelyi, D.K. Christen, R. Feenstra, C. Cantoni, A. Goyal, D.F. Lee, M. Paranthaman, P.N. Arendt, R.F. DePaula, J.R. Groves, and C. Prouteau: Low angle grain boundary transport in $YBa_2Cu_3O_{7-\delta}$ coated conductors. *Appl. Phys. Lett.* **76,** 1755 (2000).
15. D.T. Verebelyi, C. Cantoni, J.D. Budai, D.K. Christen, H.J. Kim, and J.R. Thompson: Critical current density of $YBa_2Cu_3O_{7-\partial}$ low-angle grain boundaries in self-field. *Appl. Phys. Lett.* **78,** 2031 (2001).
16. D.M. Feldmann, D.C. Larbalestier, D.T. Verebelyi, W. Zhang, Q. Li, G.N. Riley, R. Feenstra, A. Goyal, D.F. Lee, M. Paranthaman, D.M. Kroeger, and D.K. Christen: Inter- and intragrain transport measurements in $YBa_2Cu_3O_{7-x}$ deformation textured coated conductors. *Appl. Phys. Lett.* **79,** 3998 (2001).
17. N.F. Heinig, R.D. Redwing, J.E. Nordman, and D.C. Larbalestier: Strong to weak coupling transition in low misorientation angle thin film $YBa_2Cu_3O_{7-x}$ bicrystals. *Phys. Rev. B* **60,** 1409 (1999).
18. P.N. Arendt, S.R. Foltyn, J.R. Groves, R.F. DePaula, P.C. Dowden, J.M. Roper, and J.Y. Coulter: YBCO/YSZ coated conductors on flexible Ni alloy substrates. *Appl. Supercond.* **4,** 429 (1996).
19. Y. Iijima, K. Kakimoto, M. Kimura, K. Takeda, and T. Saitoh: Reel to reel continuous formation of Y-123 coated conductors by IBAD and PLD method. *IEEE Trans. Appl. Supercond.* **11,** 2816 (2001).
20. A. Goyal, D.P. Norton, J.D. Budai, M. Paranthaman, E.D. Specht, D.M. Kroeger, D.K. Christen, Q. He, B. Saffian, F.A. List, D.F. Lee, P.M. Martin, C.E. Klabunde, E. Hartfield, and V.K. Sikka: High critical current density superconducting tapes by epitaxial deposition of $YBa_2Cu_3O_x$ thick films on biaxially textured metals. *Appl. Phys. Lett.* **69,** 1795 (1996).
21. P.M. Mankiewich, J.H. Scofield, W.J. Skocpol, R.E. Howard, A.H. Dayem, and E. Good: Reproducible technique for fabrication of thin-films of high transition-temperature superconductors. *Appl. Phys. Lett.* **51,** 1753 (1987).
22. R. Feenstra, A.A. Gapud, F.A. List, E.D. Specht, D.K. Christen, T.G. Holesinger, and D.M. Feldmann: Critical currents I_c(77 K) > 350 A/cm-width achieved in ex situ YBCO coated conductors using a faster conversion process. *IEEE Trans. Appl. Supercond.* **15,** 2803 (2005).
23. J. Yoo, K.J. Leonard, H.S. Hsu, L. Heatherly, F.A. List, D.F. Lee, A.A. Gapud, P.M. Martin, S. Cook, M. Paranthaman, A. Goyal, and D.M. Kroeger: The growth of YBCO films with high critical current at reduced pressures using the BaF_2 ex situ process. *Supercond. Sci. Technol.* **17,** 1209 (2004).
24. M.W. Rupich, D.T. Verebelyi, W. Zhang, T. Kodenkandath, and X.P. Li: Metalorganic deposition of YBCO films for second-generation high-temperature superconductor wires. *MRS Bull.* **29**(8), 572 (2004).
25. T.G. Holesinger, P.N. Arendt, R. Feenstra, A.A. Gapud, E.D. Specht, D.M. Feldmann, and D.C. Larbalestier: Liquid mediated growth and the bi-modal microstructure of $YBa_2Cu_3O_{7-\partial}$ films made by the ex situ conversion of PVD-BaF_2 precursors. *J. Mater. Res.* **20,** 1216 (2005).
26. D.M. Feldmann, J.L. Reeves, A.A. Polyanskii, G. Kozlowski, R.R. Biggers, R.M. Nekkanti, I. Maartense, M. Tomsic, P. Barnes, C.E. Oberly, T.L. Peterson, S.E. Babcock, and D.C. Larbalestier: Influence of nickel substrate grain structure on $YBa_2Cu_3O_{7-x}$ supercurrent connectivity in deformation-textured coated conductors. *Appl. Phys. Lett.* **77,** 2906 (2000).
27. D.M. Feldmann, J.L. Reeves, A.A. Polyanskii, A. Goyal, R. Feenstra, D.F. Lee, M. Paranthaman, D.M. Kroeger, D.K. Christen, S.E. Babcock, and D.C. Larbalestier: Magneto-optical imaging of transport currents in $YBa_2Cu_3O_{7-x}$ on RABiTS (TM). *IEEE Trans. Appl. Supercond.* **11,** 3772 (2001).
28. A. Goyal, S.X. Ren, E.D. Specht, D.M. Kroeger, R. Feenstra, D. Norton, M. Paranthaman, D.F. Lee, and D.K. Christen: Texture formation and grain boundary networks in rolling assisted biaxially textured substrates and in epitaxial YBCO films on such substrates. *Micron.* **30,** 463 (1999).
29. F.J. Humphreys: Characterisation of fine-scale microstructures by electron backscatter diffraction (EBSD). *Scr. Mater.* **51,** 771 (2004).
30. D.M. Feldmann, D.C. Larbalestier, R. Feenstra, A.A. Gapud, J.D. Budai, T.G. Holesinger, and P.N. Arendt: Through-thickness superconducting and normal-state transport properties revealed by thinning of thick film ex situ $YBa_2Cu_3O_{7-x}$ coated conductors. *Appl. Phys. Lett.* **83,** 3951 (2003).
31. D.M. Feldmann and R. Feenstra: PVD-BaF_2 films of 0.7, 1.0 and 1.4 microns thick deposited on RABiTS substrates were studied by EBSD and all found to exhibit varying degrees of GB meander. (unpublished).
32. C. Jooss, J. Albrecht, H. Kuhn, S. Leonhardt, and H. Kronmuller: Magneto-optical studies of current distributions in high-T_c superconductors. *Rep. Prog. Phys.* **65,** 651 (2002).
33. T.H. Holesinger, unpublished (2004).
34. X.F. Zhang, D.J. Miller, and J. Talvacchio: Control of meandering grain boundary configurations in $YBa_2Cu_3O_y$ bicrystal thin films based on deposition rate. *J. Mater. Res.* **11,** 2440 (1996).
35. D.J. Miller, T.A. Roberts, J.H. Kang, J. Talvacchio, D.B. Buchholz, and R.P.H. Chang: Meandering grain-boundaries in $YBa_2Cu_3O_y$ Bi-crystal thin-films. *Appl. Phys. Lett.* **66,** 2561 (1995).
36. T.H. Holesinger, D.M. Feldmann, and R. Feenstra: Development of ex situ processed, high I_c coated conductors, in *Superconductivity for Electric Systems 2004* Annual Peer Review (Washington, DC, 2004).
37. J.H. Durrell, M.J. Hogg, F. Kahlmann, Z.H. Barber, M.G. Blamire, and J.E. Evetts: Critical current of $YBa_2Cu_3O_{7-\partial}$ low-angle grain boundaries. *Phys. Rev. Lett.* **90,** 247006 (2003).
38. S.I. Kim, D.M. Feldmann, D.T. Verebelyi, C. Thieme, W. Zhang, A.A. Polyanskii, and D.C. Larbalestier: Influence of the grain boundary network on the critical current density of deformation-textured MOD $YBa_2Cu_3O_{7-x}$ coated conductors. *Phys. Rev. B* **71,** 104501 (2005).